Zero Ripple Current With Coupled Inductors in Continuous Conduction Mode Under PWM Signals

David Gilabert, Esteban Sanchis-Kilders, *Senior Member, IEEE*, Pedro J. Martínez, Enrique Maset, *Member, IEEE*, Agustín Ferreres, and Vicente Esteve, *Senior Member, IEEE*

***Abstract*— This article presents a generalized analysis to explain current ripple of an m windings coupled inductor with a given coupling factor k_{ij} for each pair of windings and then studies more in detail its use in the continuous conduction mode and with pulsewidth modulated signals. To determine the current ripple, a generalized expression of the equivalent inductance of each winding is calculated, including the influence of voltage unbalance. In the ideal case, the equivalent inductance shows that the current ripple can only become m times smaller than that with uncoupled inductors. But in the unbalanced case, some divergences of the equivalent inductance appear that are responsible for zero ripple current. The proposed generalized expressions of the equivalent inductance also describe the current ripple of the new appearing intervals due to out-of-phase signals. An easy to design condition is proposed that achieves zero current ripple in all windings but one. Experimental results are provided that validate the presented theoretical expressions under the given conditions.**

***Index Terms*— Inductors, magnetic devices, mutual coupling.**

I. Introduction

THE coupled inductor (CI) is a widely used magnetic component in dc–dc converters.

Very common applications, such as desktop computer power supplies, use CI. In addition, volume and mass critical applications, such as aerospace and military, take advantage of CI [1]–[4]. Current ripples close to zero, which has been demonstrated to be an advantage for charging and discharging batteries in order to extend their mean life [5], also need CI. EMI reduction is also a benefit of CI as claimed in [6] and [7]. Stability of dc–dc converters is also improved when using CI [8]–[10].

Its use is also widely extended for high gain converters, but usually restricted to two winding topologies, where the classical transformer model based on leakage and magnetizing inductance is used [11]. Even though the use of CI is so extended, no generalized (more than two windings) expressions can be found in the technical literature that explain zero current ripple and sometimes their bizarre behavior (inverted current ripple, appearance of new time intervals, unexpected current slopes during these intervals, and so on).

Already, in [12]–[15], CI is used and optimized for a dc–dc converter, using reluctance models among others. But, no generalized (m windings) mathematical expressions are provided. In [14], a zero current ripple condition is given related to the coupling coefficient, k, and the turns' ratio, but the design approach is to adapt k to fulfill the zero-current condition, what is usually not easy. A very interesting study, that also includes a detailed literature review, applying a CI to an input filter with zero current ripple can be found in [16]. But, it is based on a two-winding case and the proposed expressions are, therefore, not applicable to an m winding CI.

A study in [17] proposes a current ripple reduction based on Faraday's, Ampere's, and Gauss' laws, concluding that it depends on the magnetizing and leakage inductance as well as the turns' ratio, but without providing any mathematical expression.

Other studies, such as [7], [18], and [19], reduce the current ripple, changing the duty cycle on a two-winding CI. In [20], it is concluded that, although duty cycle does not reduce current ripple, it is responsible for the sudden ripple change. Unfortunately, the study is only applicable to two windings.

The study presented in [5] is much more detailed and analyzes multiple windings but all of equal inductance. It provides expressions to find the optimum coupling to reach a zero current ripple condition for this particular case. In the experimental section, it proposes a CI with a coupling coefficient of $k = 0.2$ to reach zero current ripple. The CI will lose many of its advantages with this low value of k. In any case, the hereafter presented expressions are a general case of those provided in [5].

In [21], a very interesting analysis is done, leading to a reduced circuital model of a two-winding CI for interleaved buck converters similar to the one proposed in [22]. A generalization for more windings is also presented, but supposing all self-inductances equal and all mutual inductances equal and never overlapping the applied voltages. It also states

Manuscript received April 19, 2019; revised August 2, 2019 and August 25, 2019; accepted September 2, 2019. Date of publication September 24, 2019; date of current version November 5, 2020. This work was supported by the Spanish Ministerio de Economía, Industria y Competitividad, including a percentage from European FEDER funds, under Grant ESP2014-56169-C6-4-R and Grant ESP2016-77548-C5-5-R. Recommended for publication by Associate Editor Kai Sun. *(Corresponding author: Esteban Sanchis-Kilders.)*

The authors are with the Department of Electronic Engineering/ETSE, University of Valencia, 46100 Valencia, Spain (e-mail: esteban.sanchis@uv.es).

Color versions of one or more of the figures in this article are available online at http://ieeexplore.ieee.org.

Digital Object Identifier 10.1109/JESTPE.2019.2940848

that the current ripple is different when using CI instead of uncoupled inductors, therefore suggesting the existence of an equivalent inductance related to the coupling factor. The general expressions deduced hereafter agree with the one found in [21].

On the other side, in [6], [20], [23], and [24], some expressions are given for the equivalent inductance, ($L_{\rm eq}$), but only for the two-winding case, studying the influence of the duty cycle.

In [6, Table II], a summary of the expressions of the equivalent inductance for two-winding CI is given. But the expressions do not show any dependence with the turns' ratio, as suggested in [14].

This article first explains the analysis that leads to a generalized equivalent inductance expression, which allows to calculate the current ripple. Then, this expression is simplified and a three-winding case is analytically studied in detail, and the influence of duty, inductance ratio unbalance, and coupling coefficient is shown. A simple zero current ripple design procedure is proposed, and finally, experimental results confirm the whole theoretical analysis.

The main contribution of this article is a generalized expression of the equivalent inductance for any type of CI (as long as a common voltage can be factored out for each winding) that allows to directly deduce the current ripple of an m-winding CI. It is demonstrated that the voltage unbalance applied to the CI can be translated into a nonideal turns' ratio that explains and allows to design an m-winding CI with zero ripple current.

The analysis assumes that the design of the CI is based on a winding-voltage ratio that is equal to the square root of the inductance ratio and any deviation from this condition will be an unbalanced situation. Furthermore, it will be supposed that the CI is in the continuous conduction mode (CCM) and that its windings are excited by PWM voltage signals. Although out of the scope of this article, some of the obtained expressions could be used to extend the study to the discontinuous conduction mode (DCM). It is assumed that the dc–dc converters are usually designed to stay in a given conduction mode, either CCM or DCM. CCM is very popular among other reasons, because it is usually more stable and the transfer function is load-independent.

Parasitic resistance and capacitance will be neglected. It is expected that the parasitic resistance of the CI does not affect the study if its values are very small, which is usually the case. A study on the influence of dc resistance of the windings that justifies that it can be neglected will be presented in Section II-G. On the other hand, parasitic capacitance will limit the use of CI at high frequencies in any case and has, therefore, to be kept very small [25]. The core material is supposed to be chosen to avoid saturation and to keep permeability constant at its operating point to avoid self- and mutual-inductance change. Therefore, the study is applicable to any dc–dc converter handling PWM signals keeping the CI in CCM. Windings' phase dots can be placed in any position and this can be translated into negative coupling coefficients, k_{ij}, of the corresponding pair of windings. Out-of-phase voltage signals can also be applied and are taken into account as voltage unbalance.

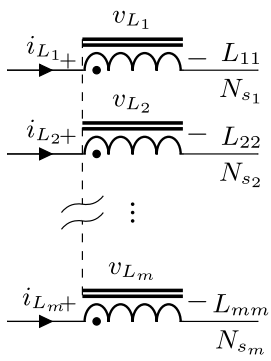

Fig. 1. CI with m windings. All self-inductances ($L_{11} \cdots L_{mm}$), turns' number ($N_{s_1} \cdots N_{s_m}$), voltages across ($v_{L_1} \cdots v_{L_m}$), and currents through each winding ($i_{L_1} \cdots i_{L_m}$) are shown. All windings are wound in the same sense on the same core.

II. Analysis of a Generalized Coupled Inductance

A. Review of the Inductance Matrix

The inductance matrix mathematically describes an m-winding CI [26]

$$\mathbf{L} = \begin{pmatrix} L_{11} & L_{12} & \cdots & L_{1m} \\ L_{21} & L_{22} & \cdots & L_{2m} \\ \vdots & \vdots & \ddots & \vdots \\ L_{m1} & L_{m2} & \cdots & L_{mm} \end{pmatrix}. \tag{1}$$

The diagonal elements are the self-inductances, $L_{\rm qq}$, and the rest of elements are the mutual inductances, $L_{\rm qr}$ (where from here on $1 \leq q, r \leq m$). The generalized Ohm's law relates currents and voltages applied to each inductance and can be written in matrix form

$$\mathbf{v_L} = \mathbf{L}\frac{d}{dt}\mathbf{i_L}. \tag{2}$$

The coupling coefficient matrix $\mathbf{k}$ is the normalized inductance matrix and can be related to (1) (see [26])

$$\mathbf{L} = \mathbf{L}_d \cdot \mathbf{k} \cdot \mathbf{L}_d. \tag{3}$$

Each coupling coefficient element, $k_{\rm qr}$, of matrix $\mathbf{k}$ describes the coupling of each pair of windings and the main diagonal elements are all equal to one, $k_{\rm qq} = 1$.

$\mathbf{L}_d$ is a diagonal matrix defined as

$$\mathbf{L}_d = \begin{cases} \sqrt{L_{\rm qq}}, & \text{if } q = r \\ 0, & \text{if } q \neq r. \end{cases} \tag{4}$$

B. Equivalent Inductance of Each Winding of a CI

As already explained in [17], [27], and [28], the equivalent inductance of each winding of a CI can be larger or smaller than the same winding alone on the core. This directly determines the current ripple measured on this winding.

Fig. 1 presents a CI with m windings. All output inductors are wound in the same sense on the same core (see phase dots). Each winding has its own self-inductance, $L_{\rm qq}$, and a number of turns, N_{s_q}. The voltage across each winding, v_{L_q}, and current through it, i_{L_q}, are also shown ($1 \leq q \leq m$).

C. Quasi-Balanced Case

A generalized inductor voltage, v'_L, can be factored out for all windings related to their turns' ratio. This will be called a quasi-balanced case. For the qth winding, this voltage is

$$v'_L = \frac{v_{L_q}}{N_{s_q}}. \tag{5}$$

Now, (2) can be rewritten as

$$\begin{pmatrix} N_{s_1} \\ N_{s_2} \\ \vdots \\ N_{s_m} \end{pmatrix} v'_L = \mathbf{L}\frac{d}{dt}\begin{pmatrix} i_{L_1} \\ i_{L_2} \\ \vdots \\ i_{L_m} \end{pmatrix}. \tag{6}$$

Equation (6) can be written in the matrix form as

$$\mathbf{N}\, v'_L dt = \mathbf{L}\cdot d\mathbf{i_L}. \tag{7}$$

A diagonal matrix of turns, $\mathbf{N}_d$, can also be defined as

$$\mathbf{N}_d = \begin{cases} N_{s_q}, & \text{if } q = r \\ 0, & \text{if } q \neq r. \end{cases} \tag{8}$$

The general equivalent inductance of each CI winding can be obtained, taking (7) to get a column vector on the left side, by left multiplying both parts by $\mathbf{L}^{-1}$ and again left multiplying by $\mathbf{N}_d^{-1}$, dividing by $v'_L dt$, and taking into account (5). The inverse of this result is also a column vector, $\mathbf{L}_{\text{eq}}$, whose elements are the equivalent inductance of each winding

$$\mathbf{L}_{\text{eq}} = \left(\mathbf{N}_d^{-1}\cdot\mathbf{L}^{-1}\cdot\mathbf{N}\right)^{-1}. \tag{9}$$

This expression, in general, applies to any CI, and it holds for any ideal and quasi-balanced case, as it already takes into account the deviation of the turns' ratio with respect to the square root of the self-inductance ratio.

Current ripple can be directly calculated with the equivalent inductance and the voltage applied in time.

D. Voltage Unbalance

Equation (7) stands for a quasi-balanced case. If a voltage unbalance exists, (9) has to be redefined. Two cases will be analyzed: in-phase and out-of-phase voltage unbalance.

1) In-Phase Voltage Unbalance: If the voltages applied to each winding are in phase but deviate from the turns' number, N_{s_q} (e.g., due to unwanted voltage drops), then v_{L_q} will not fulfill (5). To keep a constant voltage, now called v'^*_L, multiplying each winding, we define a deviation factor λ_q that relates v_{L_q} with v'^*_L and N_{s_q}

$$\lambda_q = \frac{v_{L_q}}{v'^*_L}\frac{1}{N_{s_q}}. \tag{10}$$

Using (10), we can write $v_{L_q} = \lambda_q v'^*_L N_{s_q}$ and thus modify the left-hand side of (6). The turns' number vector can be redefined as, $\mathbf{N}'^*$

$$\mathbf{N}'^* = \begin{pmatrix} N_{s_1}\lambda_1 \\ N_{s_2}\lambda_2 \\ \vdots \\ N_{s_m}\lambda_m \end{pmatrix}. \tag{11}$$

Equations (7) and (9) are valid but using now v'^*_L, $\mathbf{N}'^*$, and $\mathbf{N}'^*_d$, where the elements of $\mathbf{N}'^*_d$ correspond to (11) based on (8).

2) Out-of-Phase Voltage Unbalance: If the voltages applied to each winding are out-of-phase, v'_L of (7) is not common to all windings anymore and will become v'_{L_q}. To calculate the equivalent inductance, it is necessary to find again a common voltage, now called v^*_L, to all windings. In the case of PWM signals, delayed or not, but all with the same period, and supposing that the CI stays in CCM, the unbalance means that one winding q could be ON (see a positive voltage v_{LON_q}), and another winding r OFF (see a negative voltage v_{LOFF_r}), during a time, t_b. New time intervals appear, which will be called A_b, where $0 \leq b \leq 2^m + 1$. The number of intervals could be even larger than $2^m + 1$ if the duty of any winding q, D_q, is split. During each of these intervals, each winding will have its own equivalent inductance, L_{eq_q}.

The volt-second balance of the whole period of each winding will still apply during each interval A_b

$$v_{\text{LON}_q} D_q = -v_{\text{LOFF}_q}(1 - D_q). \tag{12}$$

To find a common voltage, v^*_L, to all windings, two functions, $f(D_q)$ and $g(D_q)$, that relate v_{Lon_q} and v_{Loff_q} with v^*_L have to be found

$$\begin{aligned} v_{\text{LON}_q} &= v^*_L\ f(D_q) \\ v_{\text{LOFF}_q} &= v^*_L\ g(D_q). \end{aligned} \tag{13}$$

Using (12), v_{LOFF_q} can be written as a function of v_{LON_q} and substituted in the second expression of (13). Then, dividing both expressions in (13), the following equation is obtained:

$$\frac{g(D_q)}{f(D_q)} = \frac{-D_q}{1 - D_q}. \tag{14}$$

Thus, a possible solution for both functions is

$$\begin{aligned} f(D_q) &= 1 - D_q \\ g(D_q) &= -D_q. \end{aligned} \tag{15}$$

The functions $f(D_q)$ and $g(D_q)$ can be unified into a single function, h, by adding another variable b_q whose value is "1" when ON voltage and "0" when OFF voltage is applied to winding q at each interval A_b. This new function is defined as

$$h(b_q, D_q) = b_q - D_q. \tag{16}$$

Therefore, each interval A_b can be described by a unique combination of m bits b_q. For example, in the case of three windings and three different duty cycles, D_1, D_2, and D_3, one combination of four intervals could be defined by its own combination of bits $b_1\ b_2\ b_3$: $A_1 \equiv b_1\ b_2\ b_3 = 111$, $A_2 \equiv b_1\ b_2\ b_3 = 011$, $A_3 \equiv b_1\ b_2\ b_3 = 001$, and $A_4 \equiv b_1\ b_2\ b_3 = 000$. Fig. 2 shows these states for a three-winding case.

So, the voltage of each winding, v_{L_q}, becomes $v^*_L N_{s_q}\lambda_q(b_q - D_q)$, where v^*_L is the common factor of all windings as in (7).

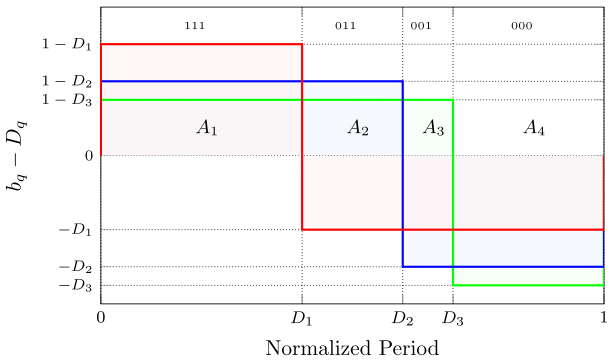

Fig. 2. Out-of-phase voltage unbalance can be caused by different ON or OFF PWM voltages applied to each winding. New intervals, A_b, can be defined, during which each winding has its own equivalent inductance, L_{eq_q}. In the case of three windings and three different duty cycles, D_1, D_2, and D_3, four intervals exist, each defined by its own combination of bits: $A_1 \equiv 111$, $A_2 \equiv 011$, $A_3 \equiv 001$, and $A_4 \equiv 000$.

The turns' ratio $\mathbf{N}'^*$ has to be redefined into $\mathbf{N}^*$ as

$$\mathbf{N}^* = \begin{pmatrix} N_{s_1}\lambda_1(b_1 - D_1) \\ N_{s_2}\lambda_2(b_2 - D_2) \\ \vdots \\ N_{s_m}\lambda_m(b_m - D_m) \end{pmatrix}. \tag{17}$$

The diagonal matrix $\mathbf{N}_d$ must also be redefined as $\mathbf{N}_d^*$

$$\mathbf{N}_d^* = \begin{cases} N_{s_q}\lambda_q(b_q - D_q), & \text{if } q = r \\ 0, & \text{if } q \neq r \end{cases}. \tag{18}$$

The equivalent inductances during each interval, A_b, of each winding can now be obtained using

$$\mathbf{L}_{\text{eq}} = \left(\mathbf{N}_d^{*-1} \cdot \mathbf{L}^{-1} \cdot \mathbf{N}^*\right)^{-1}. \tag{19}$$

This new expression (19) of the equivalent inductances will include any voltage and self-inductance unbalance and can be applied not only to a distribution like in Fig. 2 but also to out-of-phase voltages, like in interleaved PWM converters in CCM.

Equation (19) reduces to (9) when $\lambda_q = 1$ and when $(b_q - D_q)$ is the same for all windings and equal to $(b - D)$. Factor $(b - D)$ is then a common scalar to all elements of $\mathbf{N}^*$ and $\mathbf{N}_d^*$ and is simplified in (19).

E. Approximate Equivalent Inductance L_{eq}

Supposing all coupling coefficients to be the same and equal to $\tilde{k}$ allows to analytically study the behavior of $\mathbf{L}_{\text{eq}}$. This approximation introduces only a small error if all the elements of matrix $\mathbf{k}$ are very similar (apart from the diagonal elements which are all equal to one). Otherwise, a numerical analysis of $\mathbf{L}_{\text{eq}}$ using (19) has to be done.

First, the equivalent inductance of the qth output is normalized $[\overline{L_{\text{eq}_q}} = (L_{\text{eq}_q}/L_{\text{qq}})]$. Then, after operating with (19), the following simplified expression can be obtained:

$$\overline{L_{\text{eq}_q}} = \frac{[(m-1)\tilde{k}+1](1-\tilde{k})}{[(m-2)\tilde{k}+1] - \tilde{k}\sum_{\substack{r=1 \\ r\neq q}}^{m}\Delta_{\text{qr}}} \tag{20}$$

where Δ_{qr} is the deviation between the qth and rth inductors provoked by unbalances explained in Sections II-C and II-D. Its ideal value is 1

$$\Delta_{\text{qr}} = \sqrt{\frac{L_{\text{qq}}}{L_{\text{rr}}}}\frac{N_{s_r}}{N_{s_q}}\frac{\lambda_r(b_r - D_r)}{\lambda_q(b_q - D_q)}, \quad 1 \leq q,\ r \leq m. \tag{21}$$

If $\Delta_{\text{qr}} = 1$ and using (20), the ideal equivalent inductance will be

$$\overline{L_{\text{eq}_q}} = (m-1)\tilde{k} + 1. \tag{22}$$

If the coupling coefficient is one ($\tilde{k} \to 1$)

$$\overline{L_{\text{eq}_q}} \overset{\tilde{k}\to 1}{=} m. \tag{23}$$

Thus, the ideal value of $\overline{L_{\text{eq}_q}}$ when $\tilde{k} \to 1$ is the number of windings, m, of the CI and this applies to all windings. This means that the current ripple, when using CI, will ideally be reduced by a factor m but will never become zero.

F. Zero Current Ripple

Zero current ripple happens when the equivalent inductance given by (20) tends to infinity, therefore its denominator becomes zero. This point is the pole of (20)

$$\tilde{k}_{\text{pole}_q} = \frac{1}{\sum_{\substack{r=1 \\ r\neq q}}^{m}\Delta_{\text{qr}} + 2 - m}. \tag{24}$$

As $0 \leq \tilde{k} \leq 1$, only the poles in this range are a real solution. This condition can be written as

$$\sum_{\substack{r=1 \\ r\neq q}}^{m}\Delta_{\text{qr}} \geq m - 1. \tag{25}$$

Thus, the deviation Δ_{qr} is the parameter that controls the zero current ripple condition. This parameter can be changed to control the value of $\tilde{k}_{\text{pole}_q}$.

For example, if we suppose that the PWM signals applied to all windings are synchronized in time, then $(b_r - D_r) = (b_q - D_q)$. Knowing the voltage level applied to each winding and their ratio [see (10)], we could deviate from this ratio to the turns' ratio (taking into account that $L_{\text{eq}_q} \propto N_{s_q}^2$), making $\Delta_{\text{qr}} \geq 1$ and fulfilling (25). The simplified expression of Δ_{qr} applying the previous assumptions is

$$\Delta_{\text{qr}} = \frac{v_{L_r}}{v_{L_q}}\sqrt{\frac{L_{\text{qq}}}{L_{\text{rr}}}} = \frac{\sqrt{L_{\text{qq}}}}{v_{L_q}} \Big/ \frac{\sqrt{L_{\text{rr}}}}{v_{L_r}}. \tag{26}$$

If the ratio $(L_{11})^{1/2}/v_{L_1}$ is smaller than $(L_{\text{rr}})^{1/2}/v_{L_r}$ for $2 \leq r \leq m$, and $(L_{\text{rr}})^{1/2}/v_{L_r} = (L_{\text{qq}})^{1/2}/v_{L_q}$ for all $2 \leq q, r \leq m$, then $\sum \Delta_{1r} < m - 1$ for $2 \leq r \leq m$ and $\sum \Delta_{\text{qr}} \geq m - 1$ for $2 \leq q \leq m$, $1 \leq r \leq m$, and $q \neq r$. Thus, we have a pole on all windings but the first winding and can expect zero current ripple in all windings but the first winding.

If we know the coupling coefficient of all windings, we can estimate how much larger the inductance ratios have to be made to achieve the zero current ripple using (24).

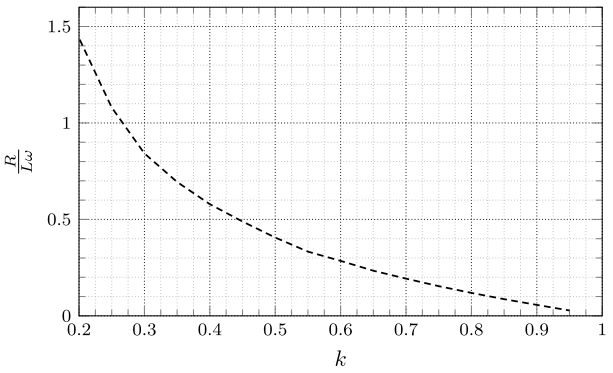

Fig. 3. Normalized resistance $R/L\omega$ with respect to coupling coefficient k in a 2×2 CI. This curve is for an error of 5% in the current slope. The switching frequency is defined by $\omega = 2\pi f_{sw}$.

G. DC Resistance Influence

It is clear that parasitic elements can influence the behavior of the CI unless they are kept very small. The parasitic elements will add to all the elements of the inductance matrix if they are ac or only the main diagonal if they are dc. The influence of dc resistance of the windings will be estimated in this section to confirm that, if their resistance is kept within reasonable values (minimum losses), the presented study is still valid.

The generalized Ohm's law in matrix form with resistance can then be written as

$$\mathbf{v_L} = \mathbf{R}\mathbf{i_L} + \mathbf{L}\frac{d}{dt}\mathbf{i_L}. \tag{27}$$

Due to the coupling effect, the resolution of the differential equations of (27) becomes very difficult, even using numerical tools.

Therefore, only the influence of the dc resistance for a 2×2 has been studied. This low order allows to calculate the current analytically with the help of specialized software tools. The deviation of the resulting current (exponential slope) compared to the ideal current (linear slope) will be used to evaluate the influence of dc resistance. A deviation of 5% will be fixed as maximum error. Both currents (the ideal and the real with a dc resistance) start at the same point (origin) but they end up in different points and 5% current difference has been used as error reference. Taking into account that the exponential behavior depends on the normalized resistance $R/L\omega$, the influence of $R/L\omega$ in the current slope with respect to the coupling coefficient, k, has been determined (ω is the switching frequency). Fig. 3 shows this influence.

Finally, to evaluate if a 5% deviation is large, the following numerical example is given. For an inductance of 66μH, a switching frequency of 100 kHz, and a coupling coefficient of $k = 0.8$, the normalized resistance is $R/L\omega = 0.12$, which means a dc resistance of $R = 5\ \Omega$. This value is too large in a usual design that wants to avoid copper losses.

Therefore, a design that minimizes losses (yielding high efficiency) will already assure that the presented expressions are applicable, because the resistances will be negligible. Fig. 3 also shows that high coupling coefficients should be avoided when using CI to reduce the influence of dc resistance.

III. Three-Winding Example

In this section, the presented equations will be applied to a three-winding case, first theoretically and, in Section IV, experimentally. The ideal and the unbalanced case will be studied. The coupling coefficient will be supposed to be the same for all windings, $\tilde{k}$. The evolution of the equivalent inductance with $\tilde{k}$ and thus the current ripple will be analyzed.

For three windings and following (20), the equivalent inductances, $\overline{L_{\mathrm{eq}_q}}$, for each winding are (28)–(30) and include the deviation factors, Δ_{qr}:

$$\overline{L_{\mathrm{eq}_1}} = \frac{(2\tilde{k}+1)(1-\tilde{k})}{(1+\tilde{k}) - \tilde{k}(\Delta_{12}+\Delta_{13})} \tag{28}$$

$$\overline{L_{\mathrm{eq}_2}} = \frac{(2\tilde{k}+1)(1-\tilde{k})}{(1+\tilde{k}) - \tilde{k}(\Delta_{21}+\Delta_{23})} \tag{29}$$

$$\overline{L_{\mathrm{eq}_3}} = \frac{(2\tilde{k}+1)(1-\tilde{k})}{(1+\tilde{k}) - \tilde{k}(\Delta_{31}+\Delta_{32})}. \tag{30}$$

A. Ideal Case: $\Delta_{\mathrm{qr}} = 1$

Taking (22) and substituting $m = 3$

$$\overline{L_{\mathrm{eq}_q}} = 2\tilde{k} + 1. \tag{31}$$

Knowing that $0 \leq \tilde{k} \leq 1$, then it is clear that $1 \leq \overline{L_{\mathrm{eq}_q}} \leq 3$ as expected.

B. Unbalanced Case: $\Delta_{\mathrm{qr}} \neq 1$

Now the equivalent inductance, $\overline{L_{\mathrm{eq}_q}}$, will be studied but considering the unbalance introduced by Δ_{qr}. First, the poles' evolution will be analyzed, because they will be responsible for divergent values of $\overline{L_{\mathrm{eq}_q}}$. Based on (24), the pole of $\overline{L_{\mathrm{eq}_3}}$ (for the other two equivalent inductances, the poles will be similar) is

$$\tilde{k}_{\mathrm{pole}_3} = \frac{1}{\Delta_{31} + \Delta_{32} - 1}. \tag{32}$$

Fig. 4 shows how the pole [see (32)], defined by $\tilde{k}$, changes with Δ_{31} and using the deviation Δ_{32} as parameter.

As an example, inductance and voltage ratios, such as $((L_{22}/L_{11}))^{1/2} = 1.81$, $((L_{33}/L_{11}))^{1/2} = 2,25$, $((L_{33}/L_{22}))^{1/2} = 1.26$, $(v_{L2}/v_{L_1}) = 1.82$, $(v_{L_3}/v_{L_1}) = 2.35$, and $(v_{L_3}/v_{L_2}) = 1.31$, have been supposed. The duty cycles are supposed to be balanced $(b_r - D_r) = (b_q - D_q)$. The inductance ratio directly appears in (21), and the voltage ratio as well, taking into account (10).

Now, all values of Δ_{qr} using (21) are calculated

$$\begin{aligned} \Delta_{12} &= \Delta_{21}^{-1} = 1.008 \\ \Delta_{13} &= \Delta_{31}^{-1} = 1.047 \\ \Delta_{23} &= \Delta_{32}^{-1} = 1.040. \end{aligned} \tag{33}$$

The poles appear for $\overline{L_{\mathrm{eq}_1}}$ at $\tilde{k}_{\mathrm{pole}_1} = 0.947$ and for $\overline{L_{\mathrm{eq}_2}}$ at $\tilde{k}_{\mathrm{pole}_2} = 0.970$, where equivalent inductances diverge. They are

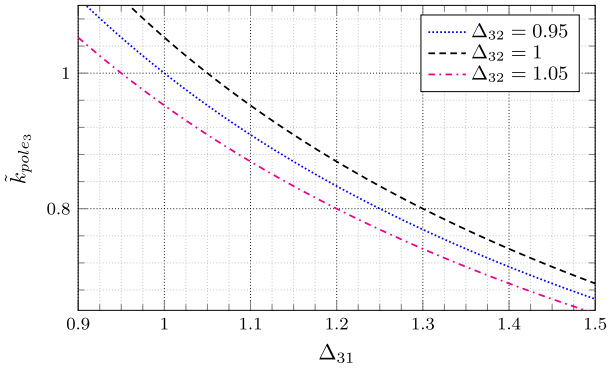

Fig. 4. Coupling coefficient value, $\tilde{k}_{\text{pole}_3}$, corresponding to the pole of $\overline{L_{\text{eq}_3}}$ and its variation with Δ_{31} using Δ_{32} as parameter. Values above 1 are not physically feasible.

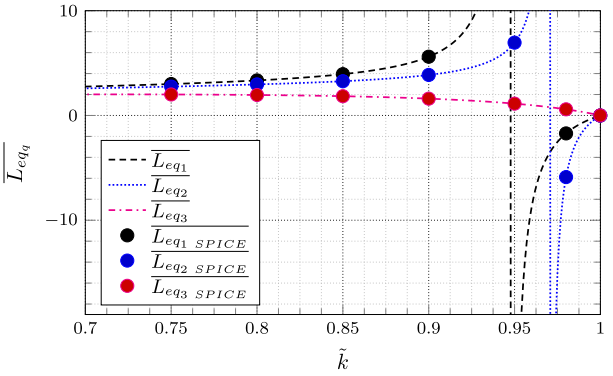

Fig. 5. Evolution of $\overline{L_{\text{eq}_q}}$ with respect to $\tilde{k}$ for $m = 3$. The deviations used are given in (33). The poles appear at $\tilde{k}_{\text{pole}_1} = 0.947$ and $\tilde{k}_{\text{pole}_2} = 0.970$. Simulation results, depicted with dots, confirm the theoretical expressions.

clearly seen when depicting (28)–(30) (see Fig. 5) as a function of $\tilde{k}$ with the calculated values of Δ_{qr} shown in (33). SPICE simulations of circuit of Fig. 6 have been done, adding square voltage sources, varying the coupling coefficient, unbalancing as required, and then measuring the equivalent inductance using the resulting current ripple. The curves are confirmed by these SPICE simulations (shown by dots), which agree with the calculated expressions.

Fig. 4 also shows that for $\Delta_{31} = 0.955$, the poles are out of the real range of $\tilde{k}$, because $\tilde{k} \in [0, 1]$. This means that the inductance $\overline{L_{\text{eq}_3}}$ would not have a pole in all the real range of $\tilde{k}$ (see in Fig. 5, the curve corresponding to $\overline{L_{\text{eq}_3}}$). On the other side, the inductances, $\overline{L_{\text{eq}_1}}$ and $\overline{L_{\text{eq}_2}}$, have poles where they tend to infinity and in these cases, their current ripple will be zero. The poles of $\overline{L_{\text{eq}_1}}$ and $\overline{L_{\text{eq}_2}}$ appear at $\tilde{k}_{\text{pole}_1} = 0.947$ and $\tilde{k}_{\text{pole}_2} = 0.970$. The pole of $\overline{L_{\text{eq}_3}}$ at $\tilde{k}_{\text{pole}_3} = 1.090$ is not a real value.

Fig. 5 also shows that for $\tilde{k} > 0.95$, the values of L_{eq_1} and L_{eq_2} can be smaller than the inductances for $\tilde{k} = 0$ or even have negative values. Negative inductance results in negative current ripple even though applying a positive voltage to the winding. Having smaller inductances (like when $\tilde{k} \to 1$) could mean that the corresponding outputs change to DCM.

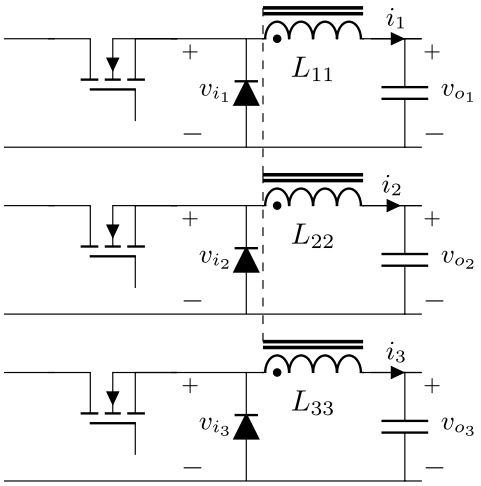

Fig. 6. Three independent buck converters with a common CI used for the experimental test.

For the particular value of $\tilde{k} \simeq 0.8$ (see Fig. 5), the equivalent inductance $\overline{L_{\text{eq}_q}}$ will be

$$\begin{aligned} \overline{L_{\text{eq}_1}} &= 3.34 \\ \overline{L_{\text{eq}_2}} &= 3.23 \\ \overline{L_{\text{eq}_3}} &= 1.97. \end{aligned} \tag{34}$$

In this case, the factor that increases the equivalent inductance is greater than the maximum ideal factor which is 3 (because $m = 3$) for two inductances and one inductance is smaller. The reason for the nonlinear behavior of L_{eq_q} are the poles generated by Δ_{qr}.

IV. Experimental Results

Two tests have been performed with the hereafter described prototype. Both tests want to confirm that the derived expressions (19) and (20) are valid, both under an unbalanced in-phase situation yielding zero-ripple current (Section IV-A) and under an unbalanced out-of-phase situation, that of course does not yield zero-ripple current anymore (Section IV-B).

For the experimental test, three different buck converters, which share a common CI, have been used.

The circuit shown in Fig. 6 shows the three buck converters and they can have different input voltages and duty cycles which allow to balance or unbalance the CI. Changing the duty cycles will also allow to test the different time intervals, A_b, and measure the resulting current slopes compared to the theoretical prediction.

The selected nominal specifications of the 100-kHz switching frequency buck converters are given in Table I. The minimum current together with the current ripple allows to determine the boundary between CCM and DCM. The nominal duty cycle is $D = 0.4$.

L_{11} can be calculated using the values given for output 1 in Table I

$$L_{11} = 66.0\ \mu\text{H}. \tag{35}$$

TABLE I
SPECIFICATIONS OF BUCK CONVERTERS SHOWN IN FIG. 6

output	v_i (V)	v_o (V)	Δi_L (A)	i_{max} (A)	i_{min} (A)
1	8.25	3.3	0.3	1.1	0.9
2	12.5	5	≤ 0.02	0.75	0.2
3	30	12	≤ 0.05	0.75	0.2

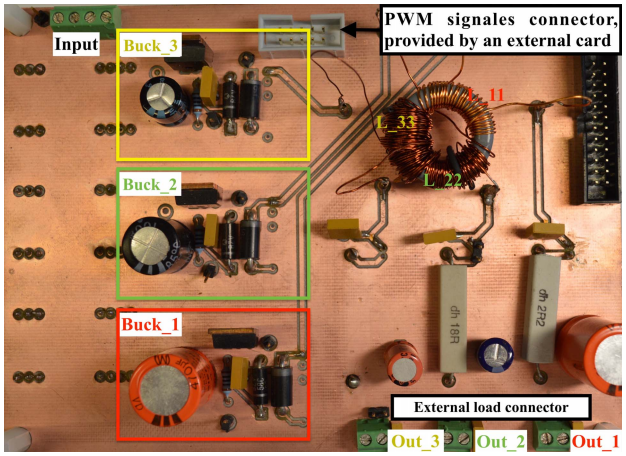

Fig. 7. Experimental prototype with the three buck converters and the common CI.

In an ideal case where $\Delta_{qr} = 1$ and using (26), L_{22} and L_{33} can be calculated

$$L_{22} = 151.5 \ \mu\text{H}$$
$$L_{33} = 872.7 \ \mu\text{H}. \tag{36}$$

But these two inductances do not fulfill the required current ripple of Table I.

The CI manufactured is wound on a toroidal core #55310-A2 of Magnetics, and as suggested in Fig. 5, a coupling coefficient of $\tilde{k} \approx 0.8$ will be designed. To do so, the three windings have been wound on the three different sectors of the toroid, not overlapping the windings, to reduce the coupling (see Fig. 8).

The built CI was measured using the network analyzer Agilent E5061B. In case the operating point of the CI changes the permeability of the core (for example, due to high dc current), the measurement has to be modified to know the inductance values under the real operating conditions (for example, biasing the CI with dc current using Agilent 42841 while measuring both self and mutual inductances). The coupling coefficient matrix has also been measured [25]. All waveform related magnitudes hereafter have been measured with oscilloscope Agilent DSO-X 3054A.

Fig. 7 shows the prototype with the three different buck converters and the common CI. Connectors provide driving PWM signals, additional loads, and input voltages.

A. Adjustment of the Inductance Ratio to Achieve an Unbalanced Case That Yields Zero Current Ripple

Because the required current ripple is not reached with the calculated inductances, a zero current ripple design is proposed, as described in Section II-F. The selection criteria of the inductance without zero-ripple current have been to choose the inductance of the output with the smallest load variation in order to assure CCM always. In our case, output 1 has the smallest load variation; therefore, the "first" inductance will be L_{11}. Other selection criteria to suit other design constraints are also possible as long as CCM is preserved in all outputs.

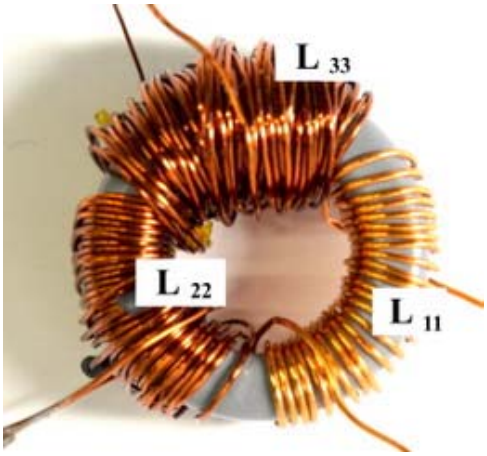

Fig. 8. CI used in the experimental setup. Notice that the three windings have been wound on three different sectors to reduce the coupling coefficient to achieve zero-ripple current.

Using the winding strategy of sector distribution that results in a coupling coefficient of $\tilde{k} \approx 0.8$, L_{22} and L_{33} have been increased in order to fulfill the following inequalities $\sum \Delta_{1r} < m-1$, $\sum \Delta_{2r} > m-1$, and $\sum \Delta_{3r} > m-1$, where $m = 3$ (the number of windings). This means that L_{11} will not have any pole, but L_{22} and L_{33} will have poles and therefore zero ripple current. By increasing L_{22} and L_{33} using (29) and (30) [an increase of approximately 35% with respect to the values given by (36)], the divergence has moved down to $\tilde{k} \approx 0.85$.

The measured, already increased, self-inductances, (37), and the coupling coefficient matrix, (38), are

$$L_{11} = 67.7 \ \mu\text{H}$$
$$L_{22} = 204.8 \ \mu\text{H} \tag{37}$$
$$L_{33} = 1191.0 \ \mu\text{H}$$
$$\mathbf{k} = \begin{pmatrix} 1 & 0.79 & 0.8 \\ 0.79 & 1 & 0.8 \\ 0.8 & 0.8 & 1 \end{pmatrix}. \tag{38}$$

Based on (19) and in an ideal case, the equivalent inductances are expected to be

$$L_{eq_1} = 81 \ \mu\text{H}$$
$$L_{eq_2} = 1500 \ \mu\text{H}$$
$$L_{eq_3} = 8692 \ \mu\text{H}. \tag{39}$$

To calculate the deviations, we take the mean value of all coupling coefficients, except the diagonal values, and verify that $\sum \Delta_{1r} = 1.74$, $\sum \Delta_{2r} = 2.14$, and $\sum \Delta_{3r} = 2.16$. This means that a divergence will appear for both L_{22} and L_{33}.

Testing this new CI, the equivalent inductances are measured (see Table II) using the applied voltages and current ripple shown in the oscilloscope (see Figs. 9 and 10).

TABLE II
MEASURED EQUIVALENT INDUCTANCES

	Interval A_1	Interval A_4
L_{eq_1} (μH)	59.4 ± 3.7	64.3 ± 3.7
L_{eq_2} (μH)	1451.4 ± 123.5	1432.0 ± 123.5
L_{eq_3} (μH)	5745 ± 662	5372 ± 662

TABLE III
EQUIVALENT INDUCTANCES USING THE MATHEMATICAL MODEL

	Eq. (19) $A_1 = A_4$	Eq. (20) $A_1 = A_4$
L_{eq_1} (μH)	66.0	65.4
L_{eq_2} (μH)	1168.7	1523.7
L_{eq_3} (μH)	5278	5894

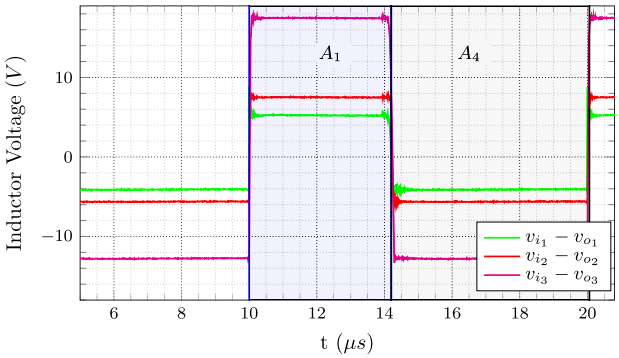

Fig. 9. Voltage waveforms applied to the three windings of the CI. Only two intervals, A_1 and A_4, exist. Interval A_1 is defined with digital word $b_1b_2b_3 = 111$ and interval A_4 with digital word $b_1b_2b_3 = 000$. The digital value 1 stands for a positive and 0 for a negative voltage v_{L_q}.

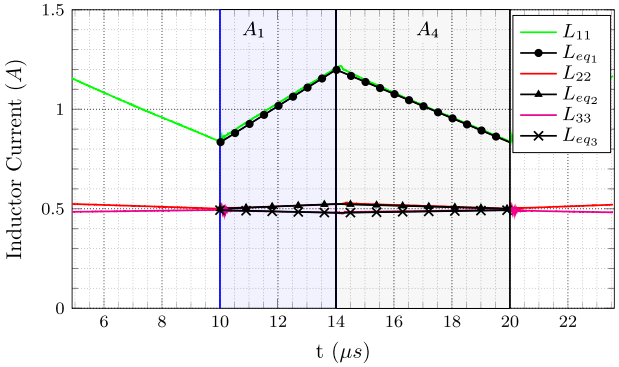

Fig. 10. Measured and calculated [dotted lines using L_{eq} in (19)] current waveforms of circuit shown in Fig. 6. Zero current ripple is almost achieved in L_{22} and L_{33} and ripple of L_{22} is larger because the value of L_{22} has decreased.

Comparing the theoretical calculations of the equivalent inductances of (19) and (20), see Table III, we see that they are very similar and the approximate expression (20) is very accurate.

Fig. 10 shows the corresponding current waveforms measured also with the oscilloscope. The current slopes have also been calculated, using (19) and the value of the measured duty cycle.

Zero ripple current can be observed for L_{22} and L_{33}. Current ripple of L_{33} seen in Fig. 10 is negative, which means that

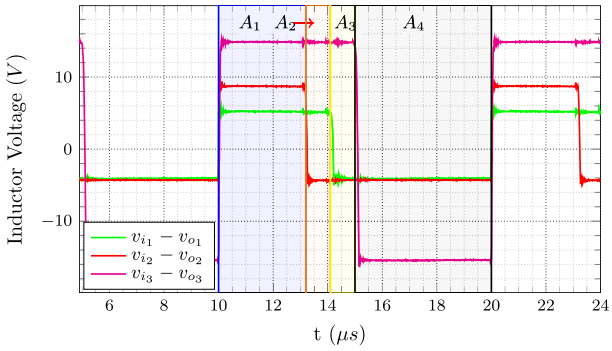

Fig. 11. Voltage waveforms with different duty cycles applied to the three windings of the CI. Four different intervals, A_1, A_2, A_3, and A_4, exist. Interval A_1 is defined by $b_1b_2b_3 = 111$, A_2 by $b_1b_2b_3 = 101$, A_3 by $b_1b_2b_3 = 001$, and A_4 by $b_1b_2b_3 = 000$, where b_1 corresponds to $v_{L_1} = v_{i_1} - v_{o_1}$, b_2 to $v_{L_2} = v_{i_2} - v_{o_2}$, and b_3 to $v_{L_3} = v_{i_3} - v_{o_3}$. The digital value 1 stands for a positive and 0 for a negative voltage v_{L_q}.

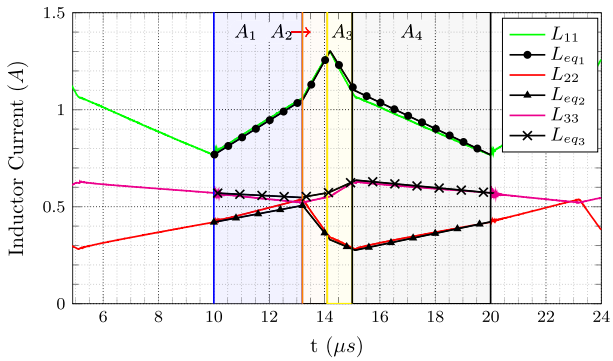

Fig. 12. Measured and calculated [dotted lines using L_{eq} in (19)] current waveforms of all intervals of circuit of Fig. 6 excited with signals shown in Fig. 11 corresponding to an unbalanced out-of-phase case.

the divergence appears at a value of k smaller than the real coupling of the windings.

B. Adjustment of the Duty Cycle That Leads to an Unbalanced Case

To confirm that the expressions that study the duty cycle unbalance, derived in Section II-D2, are correct, the duty cycles have been changed in this experiment in such a way that an unbalance with four intervals, A_1–A_4, appears. The previous experimental setup has been used but, of course, the resulting ripple will not fulfill the current-ripple specifications anymore. The three duty cycles have been made different and are

$$D_1 = 42\ \%$$
$$D_2 = 32\ \%$$
$$D_3 = 50\ \%. \tag{40}$$

As mentioned, the CI used is the same as the one described in Section IV-A, having the inductances and coupling coefficients given in (37) and (38).

Fig. 11 shows the voltage waveforms applied to each winding. Each interval will have an associated equivalent inductance, as explained in Section II-D2.

Fig. 12 shows the corresponding current waveforms measured also with the oscilloscope. The current waveforms have

TABLE IV
EQUIVALENT INDUCTANCES (a) MEASURED AND (b) CALCULATED USING THE MATHEMATICAL MODEL

a)

	A_1	A_2	A_3	A_4
L_{eq_1} (μH)	58.9 ± 2.3	21 ± 1.4	15.4 ± 1.1	65.7 ± 2.5
L_{eq_2} (μH)	245.9 ± 8.1	20.1 ± 1.4	65.3 ± 5.3	158.4 ± 6.5
L_{eq_3} (μH)	967.1 ± 73.7	499.2 ± 113.2	155.3 ± 38.5	1376.9 ± 78.1

b)

	A_1	A_2	A_3	A_4
L_{eq_1} (μH)	64.9	19.6	15.5	59.4
L_{eq_2} (μH)	236.4	20.4	56.5	138.8
L_{eq_3} (μH)	1059.0	484.6	174.8	1276.5

also been calculated based on the equivalent inductances and shown in Table IV, using (19) and therefore taking into account (17) and (18).

The reason for the difference between theoretical and measured values is mainly because the measurement of current, time, duty cycle, and voltage has been done with the oscilloscope which has limited accuracy. Fig. 12 shows that the theoretical waveforms (dotted lines) agree very well with the measured ones.

V. CONCLUSION

A generalized analysis of CI has been presented and a more detailed study when CI is in CCM and exposed to PWM signals has also been done, including ideal and unbalanced situations. Current ripple can be determined thanks to the expression of the equivalent inductance.

It has been demonstrated that, under the supposed conditions, any deviation can be reduced to a nonideal turns' ratio. Then, supposing the coupling coefficient among all windings to be the same, the generalized expression of the equivalent inductance has been simplified allowing to perform a study that has unveiled the zero ripple current conditions of CI and its relation to the described unbalance. In fact, zero ripple current condition happens only in a nonideal case and due to an unbalanced situation. General mathematical expressions have been provided to predict zero ripple current through the equivalent inductance. A design procedure to achieve zero ripple current in all outputs but one has also been proposed. This proposal that only needs to change the inductance ratio (turns' ratio) is more convenient than others found in the literature that tried to change the coupling coefficient.

Then, a three-winding case has been studied with the new approach and verified with SPICE simulation and experimental results. The analysis and test results conclude that under a balanced situation, the current ripple will be at most ($\tilde{k} = 1$) m times less compared to uncoupled inductors ($\tilde{k} = 0$). For out-of-phase unbalance, new time intervals appear, having all of them different equivalent inductances. Under an unbalanced situation, divergences can appear that can generate a zero ripple current condition and a design proposal is given. Experimental evidence confirms all analytical results.

The proposed generalized expression of the equivalent inductance agrees with other expressions found in the technical literature, which usually are only applicable to particular cases of two or three windings.

ACKNOWLEDGMENT

The authors would like to thank D. Osorno for his help in the lab and J. L. Gasent-Blesa for his support.

REFERENCES

[1] P. Pérol, "An efficient low cost modular power system for fully regulated bus in low earth orbit applications," in *Proc. 6th Eur. Space Power Conf.*, Porto, Portugal, vol. SP-502, May 2002, p. 375.
[2] G. F. Volpi, "Integrating power electronic system in space application: Limitation due to a harsh environment," in *Proc. 4th Int. Conf. Integr. Power Syst.*, Jun. 2006, pp. 1–6.
[3] H. Qunhai, Y. Jingyuan, W. Lixin, and W. Tongzhen, "Research on a new bidirectional DC–DC topology for space applications," in *Proc. IEEE Conf. Ind. Electron. Appl. (ICIEA)*, Jun. 2017, pp. 1686–1690.
[4] M. Santos, H. Ribeiro, M. Martins, and J. Guilherme, "Switch mode power supply design constraints for space applications," in *Proc. Conf. Telecommun.*, Peniche, Portugal, May 2007, pp. 157–160.
[5] T. Kang and Y. Suh, "Optimized coupling factor design of multiple-phase coupled inductor for minimum inductor current ripple operation in EV charger systems," in *Proc. IEEE 3rd Int. Future Energy Electron. Conf. ECCE Asia (IFEEC-ECCE Asia)*, Jun. 2017, pp. 1178–1183.
[6] H. Kosai, S. McNeal, A. Page, B. Jordan, J. Scofield, and B. Ray, "Characterizing the effects of inductor coupling on the performance of an interleaved boost converter," in *Proc. CARTS USA*, vol. 1, Mar. 2009, pp. 1–15.
[7] H. Liu and D. Zhang, "Design approach for coupled inductor filter in low-current-ripple input/output boost converter," in *Proc. IEEE Int. Conf. Power Renew. Energy (ICPRE)*, Oct. 2016, pp. 165–171.
[8] L. Mohammadian and E. Babaei, "Investigating the effect of inductor coupling on intrinsic stability of Cuk converter," in *Proc. 42nd Annu. Conf. IEEE Ind. Electron. Soc. (IECON)*, Oct. 2016, pp. 1359–1364.
[9] E. Sanchis-Kilders *et al.*, "Stability improvement of isolated multiple-output DC/DC converter using coupled inductors," *IEEE Trans. Aerosp. Electron. Syst.*, vol. 52, no. 4, pp. 1644–1653, Aug. 2016.
[10] Y. Yang, J. Ma, C. N.-M. Ho, and Y. Zou, "A New coupled-inductor structure for interleaving bidirectional DC–DC converters," *IEEE J. Emerg. Sel. Topics Power Electron.*, vol. 3, no. 3, pp. 841–849, Sep. 2015.
[11] H. Liu, H. Hu, H. Wu, Y. Xing, and I. Batarseh, "Overview of high-step-up coupled-inductor boost converters," *IEEE J. Emerg. Sel. Topics Power Electron.*, vol. 4, no. 2, pp. 689–704, Jun. 2016.
[12] S. Cuk and R. D. Middlebrook, "Advances in switched-mode power conversion part I," *IEEE Trans. Ind. Electron.*, vol. IE-30, no. 1, pp. 10–19, Feb. 1983.
[13] S. Cuk and R. D. Middlebrook, "Advances in switched-mode power conversion part II," *IEEE Trans. Ind. Electron.*, vol. IE-30, no. 1, pp. 19–29, Feb. 1983.
[14] S. Ćuk and Z. Zhang, "Coupled-inductor analysis and design," in *Proc. 17th Annu. IEEE Power Electron. Spec. Conf.*, Jun. 1986, pp. 655–665.
[15] S. Ćuk, "A new zero-ripple switching DC-to-DC converter and integrated magnetics," *IEEE Trans. Magn.*, vol. 19, no. 2, pp. 57–75, Mar. 1983.
[16] S. S. Nag, S. Mishra, and A. Joshi, "A passive filter building block for input or output current ripple cancellation in a power converter," *IEEE J. Emerg. Sel. Topics Power Electron.*, vol. 4, no. 2, pp. 564–575, Jun. 2016.
[17] A. F. Witulski, "Introduction to modeling of transformers and coupled inductors," *IEEE Trans. Power Electron.*, vol. 10, no. 3, pp. 349–357, May 1995.
[18] P. Shamsi and A. Shen, "Design and analysis of a class of zero fundamental ripple converters," *IEEE Trans. Power Electron.*, vol. 32, no. 6, pp. 4543–4552, Jun. 2017.
[19] S. W. Lee and H. L. Do, "Zero-ripple input-current high-step-up boost–SEPIC DC–DC converter with reduced switch-voltage stress," *IEEE Trans. Power Electron.*, vol. 32, no. 8, pp. 6170–6177, Aug. 2017.
[20] M. S. A. Jafarian and H. R. Karshenas, "Current ripple reduction in single-input, multiple-output converters using phase-shift and coupled inductors," in *Proc. 24th Iranian Conf. Elect. Eng. (ICEE)*, May 2016, pp. 816–821.

[21] G. Zhu, B. A. McDonald, and K. Wang, "Modeling and analysis of coupled inductors in power converters," *IEEE Trans. Power Electron.*, vol. 26, no. 5, pp. 1355–1363, May 2011.
[22] D. Maksimovic, R. W. Erickson, and C. Griesbach, "Modeling of cross-regulation in converters containing coupled inductors," *IEEE Trans. Power Electron.*, vol. 15, no. 4, pp. 607–615, Jul. 2000.
[23] S. A. Wibowo, Z. Ting, M. Kono, T. Taura, Y. Kobori, and H. Kobayashi, "Analysis of coupled inductors for low-ripple fast-response buck converter," in *Proc. IEEE Asia–Pacific Conf. Circuits Syst. (APCCAS)*, Nov./Dec. 2008, pp. 1860–1863.
[24] P.-L. Wong, P. Xu, B. Yang, and F. C. Lee, "Performance improvements of interleaving VRMs with coupling inductors," *IEEE Trans. Power Electron.*, vol. 16, no. 4, pp. 499–507, Jul. 2001.
[25] D. Gilabert-Palme *et al.*, "Measuring coupling coefficient of windings with dissimilar turns' number or tight coupling using resonance," *IEEE Trans. Power Electron.*, vol. 33, no. 11, pp. 9790–9802, Nov. 2018.
[26] Y. Tokad and M. B. Reed, "Criteria and tests for readability of the inductance matrix," *Trans. Amer. Inst. Elect. Eng., I, Commun. Electron.*, vol. 78, no. 6, pp. 924–926, Jan. 1960.
[27] S. Cuk, "Coupled inductor and integrated magnetics techniques in power electronics," in *Proc. 5th Int. Telecommun. Energy Conf. (INTELEC)*, Oct. 1983, pp. 269–275.
[28] J. Li, C. R. Sullivan, and A. Schultz, "Coupled-inductor design optimization for fast-response low-voltage DC–DC converters," in *Proc. 17th Annu. IEEE Appl. Power Electron. Conf. Expo. (APEC)*, vol. 2, Mar. 2002, pp. 817–823.

David Gilabert received the B.Sc. and M.Sc. degrees in electronic engineering from the University of Valencia, Valencia, Spain, in 2014, where he is currently pursuing the Ph.D. degree in complex coupled inductors.

He is also a member of the Laboratory of Industrial Electronics and Instrumentation, University of Valencia. His research interests include high-frequency magnetics, coupled inductors, and space power electronics.

Esteban Sanchis-Kilders (M'00–SM'14) was born in Valencia, Spain, in 1967. He received the M.Sc. and the Ph.D. degrees from the University of Valencia, Valencia, in 1990 and 1997, respectively.

After two years with the Power Conditioning Section, European Space Agency, Noordwijk, The Netherlands, he joined the Laboratory of Industrial Electronics and Instrumentation, University of Valencia, in 1997, where he is currently a Full Professor. His main research interests include space power electronics, magnetism, and control and industrial applications.

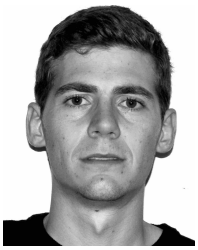

Pedro J. Martínez was born in Villarrobledo, Spain, in 1992. He received the B.Sc. and M.Sc. degrees in electronic engineering from the University of Valencia, Valencia, Spain, in 2014 and 2015, respectively, where he is currently pursuing the Ph.D. degree in reliability of gallium nitride (GaN) high-electron mobility transistors (HEMTs).

Since 2014, he has been a member of the Laboratory of Industrial Electronics and Instrumentation, University of Valencia. His current research interests include electronic power devices characterization, reliability, and space power electronics.

Enrique Maset (M'00) was born in XÃ tiva, Spain, in October 1965. He received the M.Sc. and Ph.D. degrees in physics from the University of Valencia, Valencia, Spain, in 1988 and 1993, respectively.

He is currently an Associate Professor with the Department of Electronic Engineering, University of Valencia, where he is also a member of the Laboratory of Industrial Electronics and Instrumentation. His main research interests include space power electronics and static and dynamic characterization of electronic power devices.

Agustín Ferreres was born in Sant Mateu, Spain, in 1963. He received the M.Sc. degree in physics and the Ph.D. degree in electronic engineering from the University of Valencia, Valencia, Spain, in 1993 and 1999, respectively.

For two years, he was a Power Electronics Researcher with the Research and Development Department, GH Industrial S.A., Valencia. In 1995, he joined the Laboratory of Industrial Electronics and Instrumentation, University of Valencia, where he is currently an Associate Professor. His research interests include space power electronics and industrial applications.

Vicente Esteve (M'03–SM'14) was born in Valencia, Spain, in 1961. He received the M.Sc. and Ph.D. degrees from the University of Valencia, Valencia, in 1986 and 1999, respectively.

He is currently an Associate Professor with the University of Valencia, where he is also a member of the Laboratory of Industrial Electronics and Instrumentation. He is a consultant of several electronics companies in these fields. His research interests include high-frequency rectifiers and inverters for industrial applications, and high-power inverters for induction heating.